Automatically tracking feeding behavior in populations of foraging *C. elegans*

Elsa Bonnard[1*], Jun Liu[1*], Nicolina Zjacic[1,2], Luis Alvarez[1] & Monika Scholz[1$]

1 Max Planck Research Group Neural Information Flow, Max Planck Institute for Neurobiology of Behavior – caesar, Bonn, Germany
2 Institute of Medical Genetics, University of Zurich, Zurich, Switzerland
* These authors contributed equally to this work
$ To whom correspondence may be addressed: monika.scholz@mpinb.mpg.de

Abstract

C. elegans feeds on bacteria and other small microorganisms which it ingests using its pharynx, a neuromuscular pump. Currently, measuring feeding behavior requires tracking a single animal, indirectly estimating food intake from population-level metrics, or using restrained animals. To enable large throughput feeding measurements of unrestrained, crawling worms on agarose plates at a single worm resolution, we developed an imaging protocol and a complementary image analysis tool called PharaGlow. We image up to 50 unrestrained crawling worms simultaneously and extract locomotion and feeding behaviors. We demonstrate the tool's robustness and high-throughput capabilities by measuring feeding in different use-case scenarios, such as through development, with genetic and chemical perturbations that result in faster and slower pumping, and in the presence or absence of food. Finally, we demonstrate that our tool is capable of long-term imaging by showing behavioral dynamics of mating animals over an hour. The low-resolution fluorescence microscopes required are readily available in *C. elegans* laboratories, and in combination with our python-based analysis workflow makes this methodology easily accessible. PharaGlow therefore enables the observation and analysis of the temporal dynamics of food intake and locomotory behaviors with high-throughput and precision in a user-friendly system.

Introduction

Feeding is important for animal physiology, affecting energy balance, longevity, healthspan or aging[1–3]. Accurate measurements of feeding behavior are required to assess these physiological effects. Thanks to its fully sequenced and annotated genome that shares at least 50% homology with human genome and the availability of advanced genome editing tools, short life cycle and transparency, the roundworm *C. elegans* is a powerful model to study feeding. Research in *C. elegans* has shed light on how internal states such as hunger, peptidergic and bioaminergic regulation [4–12] and decision-making affect feeding[13,14]. Being able to detect feeding in large populations, but with single-animal resolution would enable further insight into inter-animal variability, internal states and subtle modulatory effects in the temporal dynamics of feeding. Allowing animals to roam freely while feeding will enable understanding the coupling of multiple behaviors, such as locomotion and feeding, and assess both of them at the same time. Here, we propose a method to measure the feeding activity in unrestrained populations of *C. elegans* with sufficient temporal resolution to observe single feeding events.

C. elegans feeds on bacteria and other small microorganisms by drawing in a suspension of food particles from the environment. The bacteria are ingested and separated from the liquid by the pumping action of its

powerful pharyngeal muscles [15–17]. Transport of the bacteria proceeds with occasional peristaltic contractions that move food further toward the terminal bulb where a hard cuticular structure, the grinder, crushes the bacteria before they are pushed into the intestine [18]. Pumping is the limiting step for food intake i.e., the total food consumed is the product of pumping rate and external food concentration [15–17]. Pumping is inherently a stochastic process [7]. It has been suggested that stochastic pumping results from a decision-making process that serves to regulate pumping based on food availability [9]. Even in the absence of food, pumping has been observed and interpreted as a mechanism for food sampling [7,9,19] . On average, pumping occurs up to 300 times per minute when food is abundant [7,8,20]. Pumping rates are altered in response to the type, concentration, size, and familiarity of the surrounding bacteria [7,16,20,21]. The behavioral and metabolic context, such as hunger, satiety, and mating drive also influence the rate of food intake [4–6,22]. Feeding behavior is thus regulated at different time scales ranging from immediate neuro-muscular activity [19,23–25], to the intermediate scales of food choice and foraging [9,13,26], to longer-term life history traits and behavioral state changes of the animal [4,27].

Because of the transparent body of *C. elegans*, the pharynx can be directly observed through light microscopy, which in principle enables simultaneous detection of food particles (bacteria), muscular motion, and locomotion [17]. However, these experiments are often performed in immobilized animals, which can introduce artifacts in the observed behavior, as the activity of the body wall muscles feedbacks to the pharynx via parallel synaptic and hormonal routes [28,29]. While desirable, imaging feeding in unconstrained animals, especially in large populations, is challenging due to the disparate time- and length scales of the motions involved. While worms move over centimeters within minutes [30,31], the observable pharyngeal contractions are over µm within ms [17], making large scale foraging experiments technically challenging.

Existing techniques to measure feeding fall broadly into two categories. The first focuses on indirect measures of population food intake, and the second detects each pumping contraction (Table 1). Indirect food intake measures rely either on labeling the food intake of the worm, for example using bioluminescent bacteria [32], fluorescent bacteria [6,33] or fluorescent beads [17,34], or by measuring the remaining food concentration over time in large liquid cultures of worms [35]. However, liquid culture neither allows direct measure of pumping activity nor of feeding related behavior such as locomotion toward food. Resolving single pump information can be achieved by combining bright-field microscopy with live worm tracking to remove center of mass motion and enable imaging of the grinder [26,27,36], or alternatively by constraining animals in microfluidics. In tracking and constrained configurations, one can read out pumps by directly following the grinder motion in the pharynx [7,20]. A complementary technique relies on recording electropharyngeograms that detect the signature of muscular contractions in a small population of constrained animals without requiring a tracking microscope [37]. Despite these numerous approaches, what is lacking is a method that allows time-resolved pumping detection in large populations of unrestrained crawling animals.

We wanted to fill the gap to allow imaging of pumping activity at high-throughput with single-pump temporal resolution in unrestrained animals, while using only optical setups already available in most *C. elegans* laboratories. Our method is based on epi-fluorescence microscopy of the pharyngeal muscle with a cost effective, large chip camera that enables imaging of many worms as they explore freely on an agarose plate. We determined that the method is relatively insensitive to the optical instrument used, and does not require high-end or custom optics. The accompanying analysis software (PharaGlow) is written in Python and can be accessed using beginner friendly semi-graphical jupyter notebooks. PharaGlow is available under a permissive open source license. We demonstrate the usability and throughput of the method for multiple use cases, including those not previously possible in restrained animals, such as repeated imaging of a population of developing animals and investigating the coupling of locomotion and pumping rates. Finally, we demonstrate the utility of our approach by imaging a pair of mating animals over the course of more than one hour.

Table 1: Comparison of classes of automated methods for pumping analysis

Technique	Single pump	Single worm	Animals/ setup	Method	Label	Constrained	Source
Bioluminescent bacteria	No	No	100-1000	Microscopy	No	No	[32]
Luciferase expressing worms	No	Yes	100	Microscopy	Yes	No	[38]
Optical density	No	No	100-1000	Absorption	No	No	[35]
Tracking microscope	Yes	Yes	1	Microscopy	No	No	[26,27,36]
pWarp	Yes	Yes	4	Microscopy	No	microfluidic	[20]
NemaChip	Yes	Yes	8	Electrophysiology / EPG	No	microfluidic	[37]
Manual counting	Yes	Yes	1	Microscopy	No	No	[8,39,40] and many others
PharaGlow	**Yes**	**Yes**	**1-50**	**Microscopy**	**Yes**	**No**	**This paper**

RESULTS

1. Detection of pumping rates in crawling animals

To enable automated, high-throughput detection of pumping in animals crawling on culture plates, we combined epi-fluorescence microscopy with a large area scan camera (Fig. 1A). Typically, pumping is detected by manual or automated counting using high magnification to resolve the motion of the grinder in the terminal bulb [39,40]. Using animals expressing a fluorescent protein in the pharyngeal muscle allowed us

to image at a lower magnification compared to the resolution required for bright-field imaging of the grinder. Specifically, we image animals expressing YFP under the pharyngeal myosin promoter *myo-2p* (*gnaIs1 [myo-2p::yfp]*), which is present in all pharyngeal muscles except pm1 and pm2 [41,42].

By using a low magnification of 1x, we could image a field of view of 7 by 5 mm, corresponding to multiple body lengths of the worms (Fig. 1A). We simultaneously imaged tens of animals (typically 30-50) as they crawled and analyzed their behavior off-line using our custom analysis software (Fig. 1B; Video 1). The analysis pipeline combines a particle-tracking workflow with custom shape-segmentation of the fluorescent pharynx (Fig. 1C). After detecting and tracking the pharynges in the field-of-view, the contour and centerlines are fitted. The centerline and width are used to virtually straighten the animal (Fig. 1D). We then extract a pump metric from the straightened images based on the standard deviation of the fluorescence along the dorsal-ventral axis (DV-axis) of the animal, which reflects pumping events (Fig. 1E, F). By averaging images during these putative detected pumping events, we determined that this metric is sensitive to the opening of the pharyngeal lumen and contraction of the terminal bulb and thus indeed corresponds to pumping events (Fig. 1G).

Although the low magnification (1x) we use to image the animals allows us to increase the number of observed animals, this could compromise pumping detection. To determine how accurate our software detects pumping in these imaging conditions, we compared the results of our automated method and a manual annotator. Since manual annotation of pumping rates is still widely used, but practiced at higher magnifications, we simultaneously imaged worms at a magnification of 10x (pixel size 240 nm/px) in bright-field and fluorescence (Fig. 1H; Video 2). A human expert counted pumps in the videos acquired using the bright-field channel. We then ran our automated analysis on the video acquired on the fluorescence channel, but downscaled to 1x (pixelsize 2.4 µm/px). We found that PharaGlow was able to accurately detect pumping in these videos and the resulting rate and counts were in agreement with the human expert. Both methods result in a comparable mean pumping rate for the animals counted (Fig. 1I), with a deviation between the human and automated results of less than 2 pumps per 10 s (Fig. 1J). To score a typical experiment of 30 animals over 5 minutes of recording time, the human experimenter would need, at best, to count for at least 150 min of data (real time). This time is regularly longer, as accurate counting often requires scrutinizing the recordings in slow motion or visualizing the same part of the recording several times. PharaGlow is therefore able to automatically and reliably detect pumping in low-resolution, large field-of-view images, enhancing the number of animals which can be scored simultaneously.

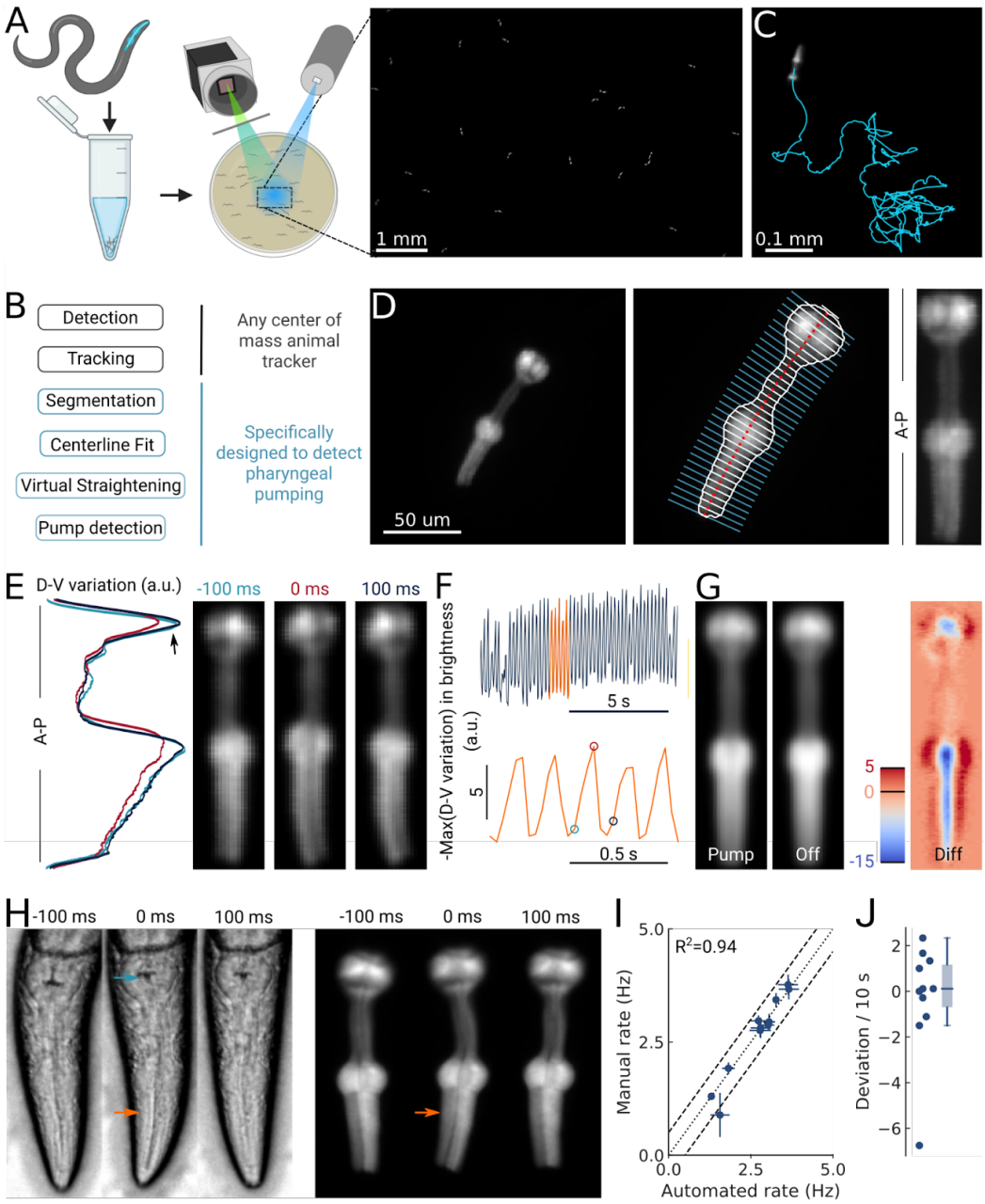

Figure 1. High-throughput optical detection of pharyngeal pumping in moving worms
(A) Hundreds of animals expressing *myo-2p::YFP* are washed in M9 and pipetted onto the assay plate before imaging with an epifluorescence microscope at 1x magnification resulting in a full field of view of 7 by 5 mm. (B) Workflow of using the PharaGlow image analysis pipeline. Animal center of mass tracking can be substituted with any available tracker, but subsequent steps are specific to tracking pumping. (C) Representative trajectory of an animal after tracking. (D) Processing steps followed for detection of pharyngeal pumping. Example of a fluorescent image (left; 2x magnification). Segmentation of pharyngeal contour, centerline, and widths (middle) calculated for virtual straightening along the anterior-posterior axis (A-P) and the resulting straightened animal (right). (E) Three straightened frames of an animal before, during, and after a pump and their dorso-ventral variation in brightness along the A-P axis. (F) The metric that is used to detect pumping events. Bottom, a portion of the top trace (orange). Highlighted time points correspond to the images in (E). (G) Average of all images during a detected pump ('Pump') and for all remaining timepoints ('Off'). The difference image ('Diff') shows that pumps are characterized by the opening of the lumen and terminal bulb contraction. Colorbar indicates brightness difference (a.u.). (H) Example image sequence of a pharynx recorded at 10x using bright-field (left) and in epi-fluorescence (right) microscopy before, during, and after a pump. Arrows denote changes in the terminal bulb (cyan) and corpus (orange). (I) Correlation between the average pumping rates for the expert annotator and PharaGlow (N = 11). (J) Deviation of the number of events between the expert and PharaGlow as the number of events in 10 s, a typical time period used in manually counted experiments.

2. Developmental pumping

Having developed this new high-throughput method which enables accurate measurements of many animals simultaneously, we wondered how pumping changes over the course of development, where the animal changes its size and its energy needs. During development, the pharynx grows with the body [43], but the ratio between pharynx and body length decreases from L1 stage to adulthood [16]. To investigate how pumping rates change during development, we imaged cohorts of synchronized worms consecutively over three days in the middle of each of the four larval stages and as young adults. Animals were imaged directly on their culturing plates while moving freely in the field of view (Fig. 2A). We accounted for the growing pharynx by adapting the magnification of our imaging system to achieve approximately the same spatial sampling of the pharynx at each stage (Fig. 2B). Under these conditions, we were able to sample at least 150 trajectories per developmental stage. Altogether, more than 1000 animal tracks remained after filtering animals that spend less than one minute in the field-of-view. Filtering leads to over-proportionally reducing young adult trajectories since these animals traverse the field of view quickly despite the spatially proportional scaling. Nevertheless, we obtain large samples of animals due to new animals continually entering, with a total measured time of four animal-hours for the adult stage, and more than 10 animal-hours for the L1 stage. The average track duration is well over one minute with 1.9 ± 0.9 minutes (mean ± s.d.) for L1 and 1.6 ± 0.6 min for adults (Fig. S2.1). These data represent two orders of magnitude more single worm pumping data than is obtainable with conventional methods (see Table 1).

We find that on-food pumping rates increase slightly over the course of the larval stages, but much less dramatically than the velocity increases over development, despite the substantial growth of both the body and the pharyngeal muscles (Fig. 2C-F). Owing to time resolution and the large number of individual worms that can be analyzed using PharaGlow, it is possible to generate smooth probability density functions of pumping across the different larval stages (Fig. 2G). A small fraction of animals did not show pumping during our recording (Fig. 2H, 5 animal tracks in L1 with < 0.5 Hz, < 1% for all other conditions). We wondered if we had captured animals during lethargus, the period of sleep preceding each molt despite choosing the imaging time points in the middle of each larval stage and working with an age synchronized population. However, lethargus is incompatible with the observed velocities of these animals. Alternatively, it is possible that these animals transiently show satiety quiescence, which might be absent under these conditions in the larger YA [6,44,45].

As we image unconstrained animals, we can simultaneously assess pumping and locomotor behaviors. Animals move forward on agar by generating waves of muscular contraction through their body. When the animals reverse the direction of these waves, they move backwards. Such spontaneous reversals are rare events, but can be triggered by diverse stimuli, such as nose touch [46] or heat [47]. The reversal rate depends also on the food condition and the developmental stage of the animal. In the absence of food, the reversal rate is higher in young adults than in larvae (about 45 events vs 30 events in 10 min), but constant throughout larval development [48]. In our on-food measurements, we find some significant differences in

reversal rates, however, the effect size is small (e.g. corresponding to a rate of 47 versus 49 pumps/10 minutes between L2 and L3 animals). The only strong difference appears between the earlier larvae L1-L3 and the later L4/young adult stages with a difference of approximately 10 reversals /10 minutes (Fig. S2.2).

We investigated whether extended exposure to light might affect worm behaviors by monitoring the amount of reversals, pumping rate, and speed. Our results suggest that there is a mild light avoidance reaction (5-25%) which depends on the developmental stage (Fig. S2.3). Repeated exposure did not affect behavior in most developmental stages, except for the young adult stage, for which a higher velocity was observed when exposed to light multiple times (Fig. S2.4). Additionally, we tested whether light exposure caused phototoxic effects. Long-term exposure (up to five hours) did not affect worm viability. Lastly, different excitation light did not affect the pumping rate, but had a mild impact on velocity (Fig. S2.5) (see Appendix for details).

Overall, we find that our imaging approach can be adapted to larvae by increasing the magnification, and our analysis pipeline is capable of handling data from hundreds of animals. While there are small deviations between the automated detection and human counted data (Fig. S2.6), we accurately detect both mean and individual rates for all stages, with a median of error between experts and our method of less than 10%. Over the course of three days and five imaging sessions, more than 1000 animals were tracked, significantly more than can be achieved with comparable methods (Table 1).

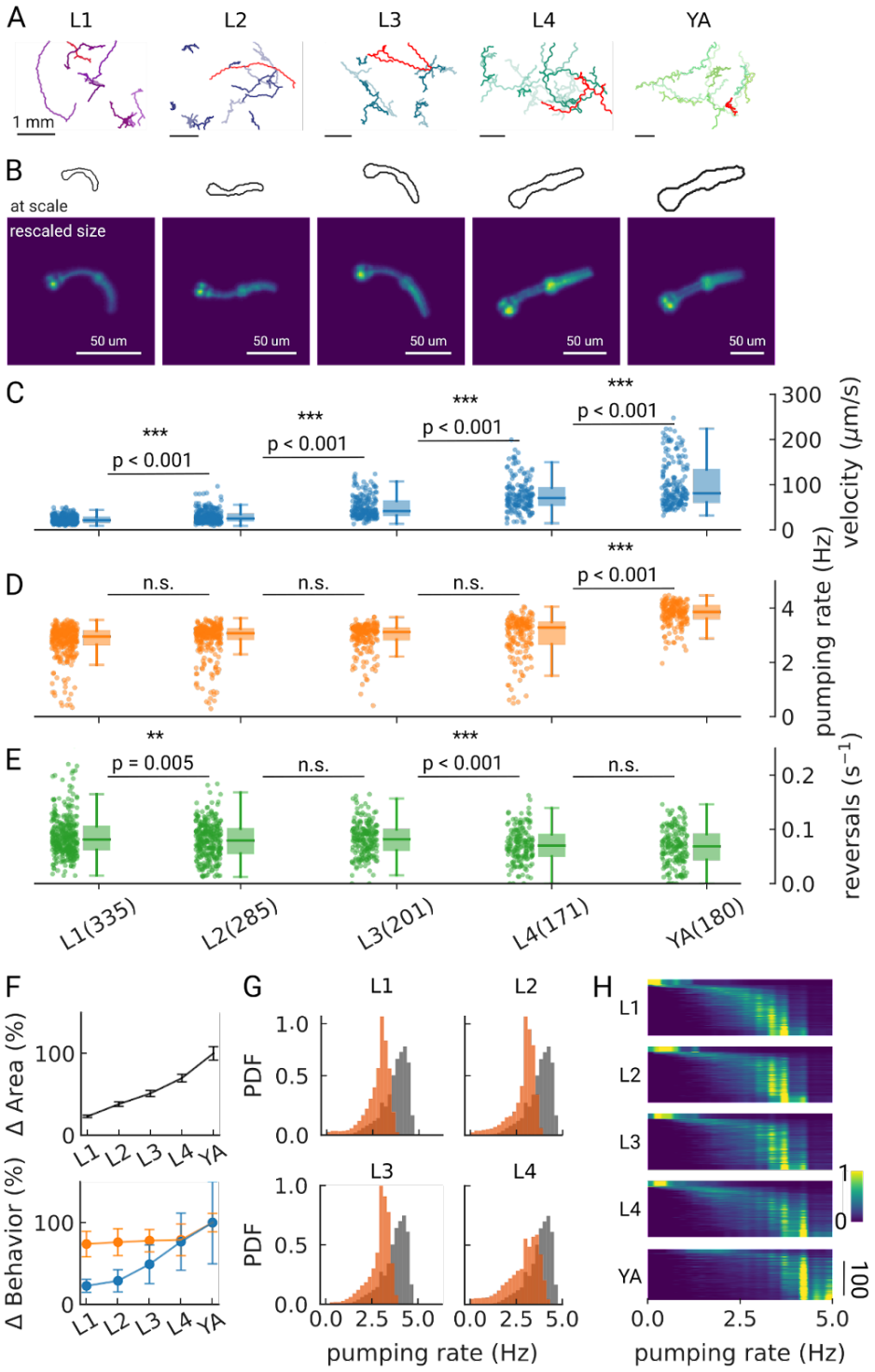

Figure 2. Changes in pumping and locomotion behavior during larval development
(A) Trajectories of 10 randomly selected animals at different larval stages (L1-L4) and young adults (YA). All scale bars correspond to 1 mm (top). (B) Size of the larvae and YA at the same scale (outlines, top) compared to the equal sizing achieved by adjusting the magnification (bottom). The image corresponds to the red track from (A). (C-D) time-averaged mean velocity (C), (D) mean pumping rate, and reversals (E) for all animals. The boxplots follow Tukey's rule where the middle line indicates the median, the box denotes the first and third quartiles, and the whiskers show the 1.5 interquartile range above and below the box. The number of tracklets per developmental stage are shown in (E), with N = 6 independent replicates per condition. (F) Relative change in the animal's area compared to the mean area of the YA stage (top) and relative change in velocity (blue) and pumping rate (orange) across development compared to the mean of the YA stage (bottom). Error bars denote s.d. (G) Pumping rate distribution for all larval stages as calculated by counting pumping events in a sliding window of width = 10 s and combining data from all animals of the same stage. The YA pumping rate distribution is underlaid in gray. (H) Pumping frequency distribution of individual worms for different developmental stages and YA.

3. Food intake is modulated by starvation

Next, we wanted to determine if our method was robust to changes in locomotion and plate context, allowing a wider range of applications such as investigating starvation or different pharmacological treatments without the presence of a bacterial food source. Off-food locomotion is faster [49,50] , and pumping irregular [7,51] , which could potentially be more challenging for detecting pumping. Prior work showed that pumping rates off food are lower, but increase over the course of starvation and that this increase is mediated by a cholinergic pathway [5]. We track animals either on-, or off food over an increasing amount of starvation time and extract behavioral dynamics (Fig. 3A-D). We confirm that pumping is dependent on the starvation duration, with a reduction in pumping rate over the course of three hours (Fig. 3B,D). Beyond the first time point, our data are consistent with prior data [5], showing a sustained rate of around 2-2.5 Hz (Fig. 3E). Previously, rates measured immediately after transferring worms off food (<30 min of starvation) were very low, possibly due to a lasting pumping suppression after harsh touch [52], which we avoid by washing worms off plates instead of picking (see Methods).

As we are able to measure pumping and locomotion behaviors simultaneously, we wanted to see if we could observe co-regulation of locomotion and feeding off-food. When taken off of food, *C. elegans* displays a restricted area search (local area search) which is characterized by frequent turns and reversals and an elevated speed [50,53–55]. This behavior lasts between 30 - 60 min, after which animals switch to longer runs that cover more area, which is a strategy for dispersal [53,56]. Interestingly, for starved worms at 30 and 90 min, the joint distribution of pumping rates and velocities show distinct sub-populations (Fig. 3F). For longer starvation durations, the population becomes homogeneous with a well-defined mean pumping rate and speed. For the shortest starvation time point we sampled, we see a mixed population with distinct speeds and pumping rates, possibly reflecting some animals that are still performing a local search and others that are not. This is consistent with the fact that these distinct populations are not apparent in worm populations that stay on food (Fig. S3.1).

To further investigate whether these groups arise from individual animals switching between distinct behavioral states or whether these distributions reflect a mixed population, we analyzed the pumping rate distributions of individual animals (Fig. 3G). Here we report the instantaneous pumping rate for each animal, which highlights regular versus irregular pumping intervals (see Methods for pumping rate calculations). Taken together, the data suggests that at 30 min starvation, a fraction of the animals show low speeds and pumping rates, and the remainder are in a high-speed, high pumping state (Fig. 3F, G). With increasing starvation time, this subset of animals decreases until all animals show similar pumping rate distributions with an average of ~ 2Hz. This result highlights the strength of PharaGlow to produce large animal statistics while preserving single worm behavioral information.

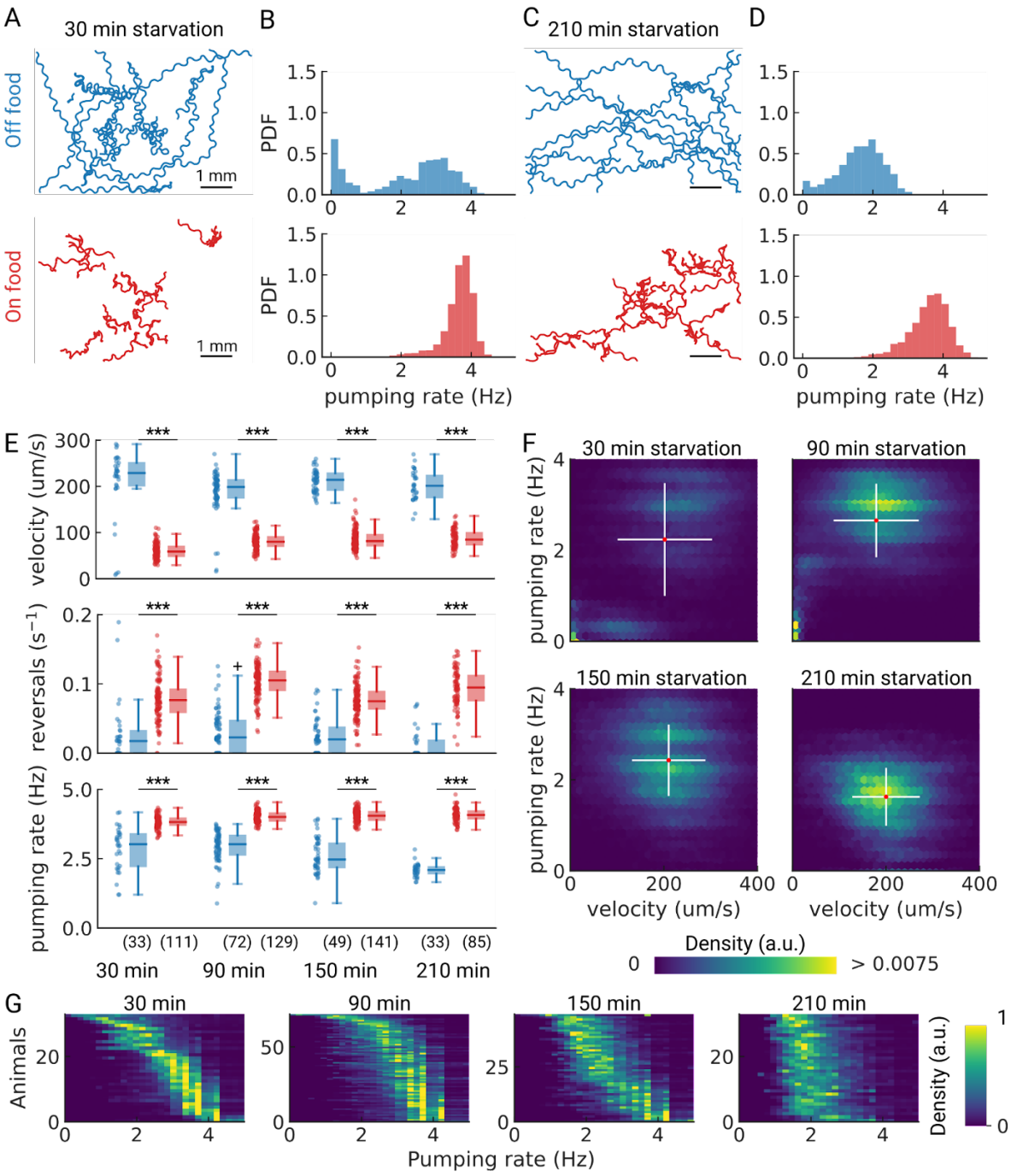

Figure 3 Pumping is modulated by starvation

(A) Example trajectories of worms after 30 min starvation (blue) or 30 min continuously on food (red), N = 10. (B) The pumping rate distributions for the conditions in (A) for all animals ($N_{starved}$ = 33, N_{onFood}= 111). (C) Same as (A) but for animals starved, or kept on food for 210 min. (D) The pumping rate distributions corresponding to (C; $N_{starved}$ = 33, N_{onFood} = 85). (E) Velocity, reversal rate, and pumping rate for animals starved and on-food controls. The sample size is given in the bottom panel. *** indicates p<0.001 (Welch's unequal variance two-tailed t-test). The sample size is given in parentheses in the bottom panel. (F) Joint distribution of velocity and pumping rate for increasing starvation times. The cross indicates the mean (red) and standard deviation (white). The density is normalized by sample number. (G) Distribution of instantaneous pumping rates for each animal (tracklet). Rows are sorted by the mean pumping rate to aid visualization.

4. Feeding mutants

A desired capability for a high-throughput feeding tool is the ability to faithfully detect pumping rates in mutant animals which might have different pharyngeal contraction patterns and body motion, potentially increasing the difficulty of detecting pumping events. To determine if PharaGlow could faithfully detect pumping and locomotion in mutant animals, we wanted to assay a range of feeding and locomotion phenotypes. We therefore selected mutants with reported constitutively high (*unc-31*) or reduced (*eat-18*) pumping rates and different locomotory patterns [23,24,57]. UNC-31 is involved in dense-core vesicle release, and *unc-31* mutant animals display reduced, uncoordinated locomotion on food (Fig. 4A). We confirm that *unc-31(e928)* and *unc-31(n1304)* animals pump at rates comparable to wildtype. However, we see a bimodal distribution of rates with a fraction of animals showing markedly lower rates (Fig. 4B). By looking at the individual animals' pumping rates, we find that *unc-31* animals show long pauses in pumping, unlike wt animals (Fig. 4F).

In contrast to *unc-31*, *eat-18* mutant animals have no previously reported locomotor defects, but pump slower than wildtype [24]. EAT-18 is expressed in the pharyngeal muscle and interacts with a nAChR subunit EAT-2 to form a functional acetylcholine receptor [23,58]. Feeding impaired mutants were previously reported to have reduced body lengths and widths [59]. As expected, we found that *eat-18* animals were smaller (Fig. 4C) and developed more slowly (approximately 91 hours from egg to adulthood compared to 63 hours for wildtype). While we detected pumping events at an average rate of 1 Hz, the animals showed a different contraction pattern and timing than either *unc-31* or wt animals (Fig. 4D, E). We confirmed that *eat-18(ad820)* animals lack the ability to perform fast pumping bursts (Fig. 4B,F) and the duration of a pharyngeal contraction is approximately doubled compared to wt (Fig. 4E, S4.1 Video 3). We do observe a higher pumping rate than previously reported for *eat-18*, where animals were reported to rarely pump during experiments (< 0.5 Hz, [23,24]). To verify that the detected motion is pumping and not peristaltic movements or other non-pharyngeal muscular motion, we verified the rate by inspecting individual videos. When verifying these sample animals, we did observe slow pumping bursts at the 1-2 Hz rates indicated by PharaGlow, suggesting that these animals are able to pump at this frequency (Fig. 4E, arrows and Video 3). We also found that *eat-18* animals showed significantly fewer reversals than wildtype, indicating a role for the nAch receptor in modulating reversals. This is likely mediated by extrapharyngeally located neurons, since *eat-18* is reported to show expression not only in the pharyngeal muscle, but also in some unidentified somatic neurons [24].

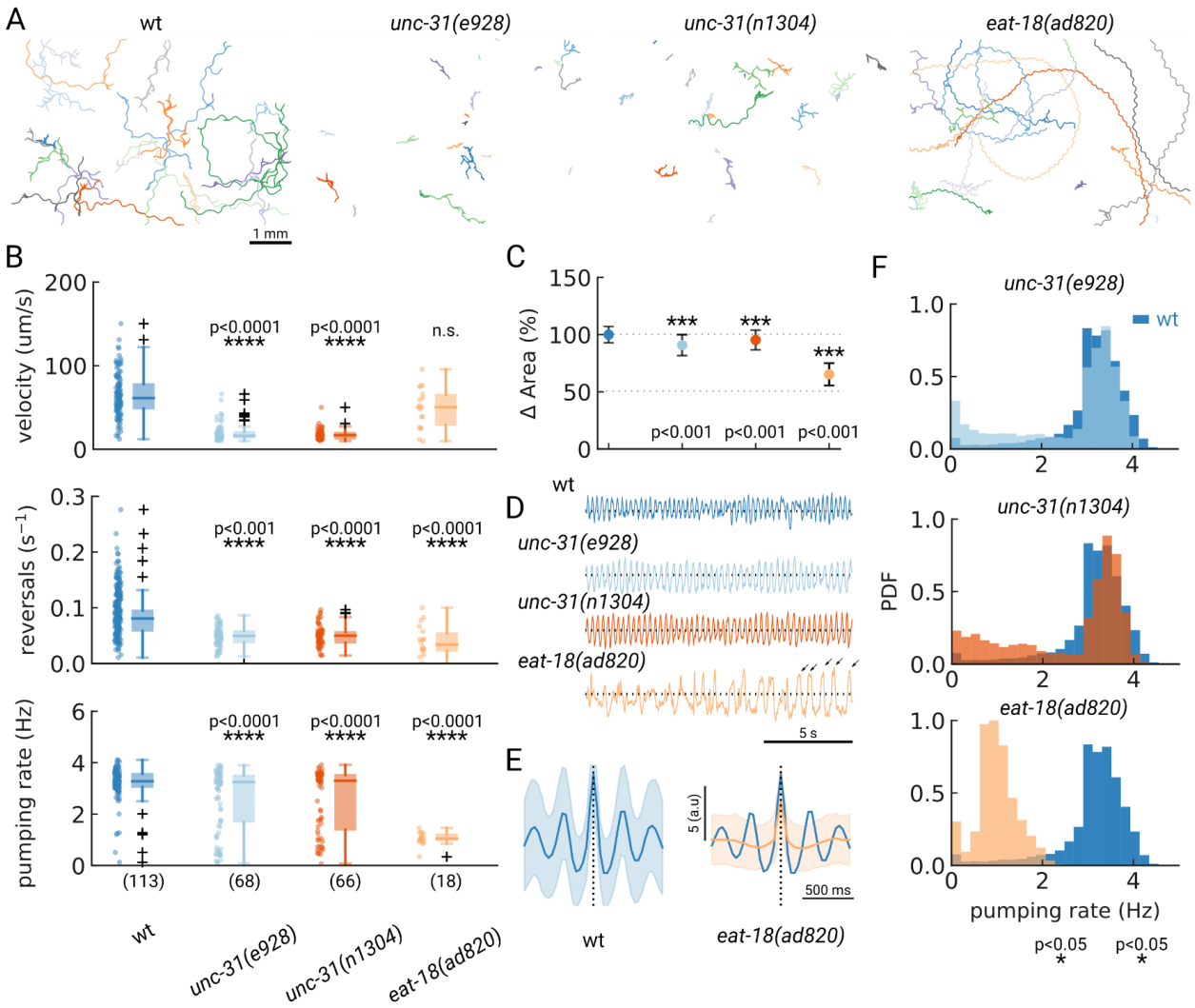

Figure 4 Automated pumping detection in feeding mutants

(A) Example trajectories of tracked animals (N = 20, except N = 18 for *eat-18(ad820)*). (B) Velocity, reversal rate and pumping rate for all genotypes. The sample size is given in parentheses in the bottom panel. (C) Mean and standard deviation of the pharyngeal areas relative to wt. (D) Pumping metric for a representative sample animal per genotype. Arrows in the *eat-18(ad820)* trace denote slow contractions. (E) Average peak shape of the pumping signal for wt (blue) and *eat-18(ad820)* (orange). The shaded area denotes s.d. (F) Pumping rate distributions. The wt pumping rate distribution is underlaid in dark blue. Significant differences between a mutant and wt are indicated as ** (p<0.01) and *** (p<0.001), all significant p-values were p<0.0001 (Welch's unequal variance two-tailed t-test).

5. Long-term recording of mating animals

Having established that PharaGlow can robustly detect locomotion and pumping behaviors across a range of conditions, we wanted to test if it is a suitable tool for long-term recordings. As a proof-of-principle, we imaged the interactions of a male and a hermaphrodite over the course of 74 minutes at 30 fps (Fig. 5A, B). As the resulting data volume would have been prohibitive, we implemented a live segmentation method that allowed us to only store the animals coordinates and the region of interest around each animal (Video 4; Methods). We then calculated the distance between the animals, allowing us to identify mating events (Fig. 5C, D). We find that the animals frequently interact over the course of 1h with multiple close encounters (Fig. 5D). The male also showed a long period of quiescence in both locomotion and pumping rate. Overall, the animals are closer at the beginning of the recording, but later spend time at larger distances (Fig. 5E, left and right panels). Despite the long imaging duration, we still observe pumping at the end of the recording, indicating that we have sufficient signal remaining to detect pumping events. We confirm this observation by calculating photo-bleaching curves. We find that the decay time of the signal is 410 ± 47 min (Fig. S5.1), which indicates that it is possible to do continuous imaging over multiple hours. In our case, the recording was limited by the male escaping the enclosure, rather than loss of signal.

Having this multi-scale data allows observing both large-scale structure and smaller events in the data. We further examined the mating event displayed in Fig. 5C. During the encounter, the male shows a larger velocity and performs many long reversals when the animals are close, as is typical for a mating attempt. It is also interesting to note that pumping does not completely cease during the attempt (Fig. 5F). Despite being in the same arena, and covering most of the enclosure during the recording (Fig. 5B), the velocity and pumping distributions differ strongly between the two animals (Fig. 5G, H). While the distributions of the male are dominated by the long quiescence period, the hermaphrodite overall shows a bi-modal rate distribution with some infrequent pumping at 4 Hz. PharaGlow is therefore able to track behavior over more than an hour, and keep the identity of animals given that these are constrained to the field-of-view.

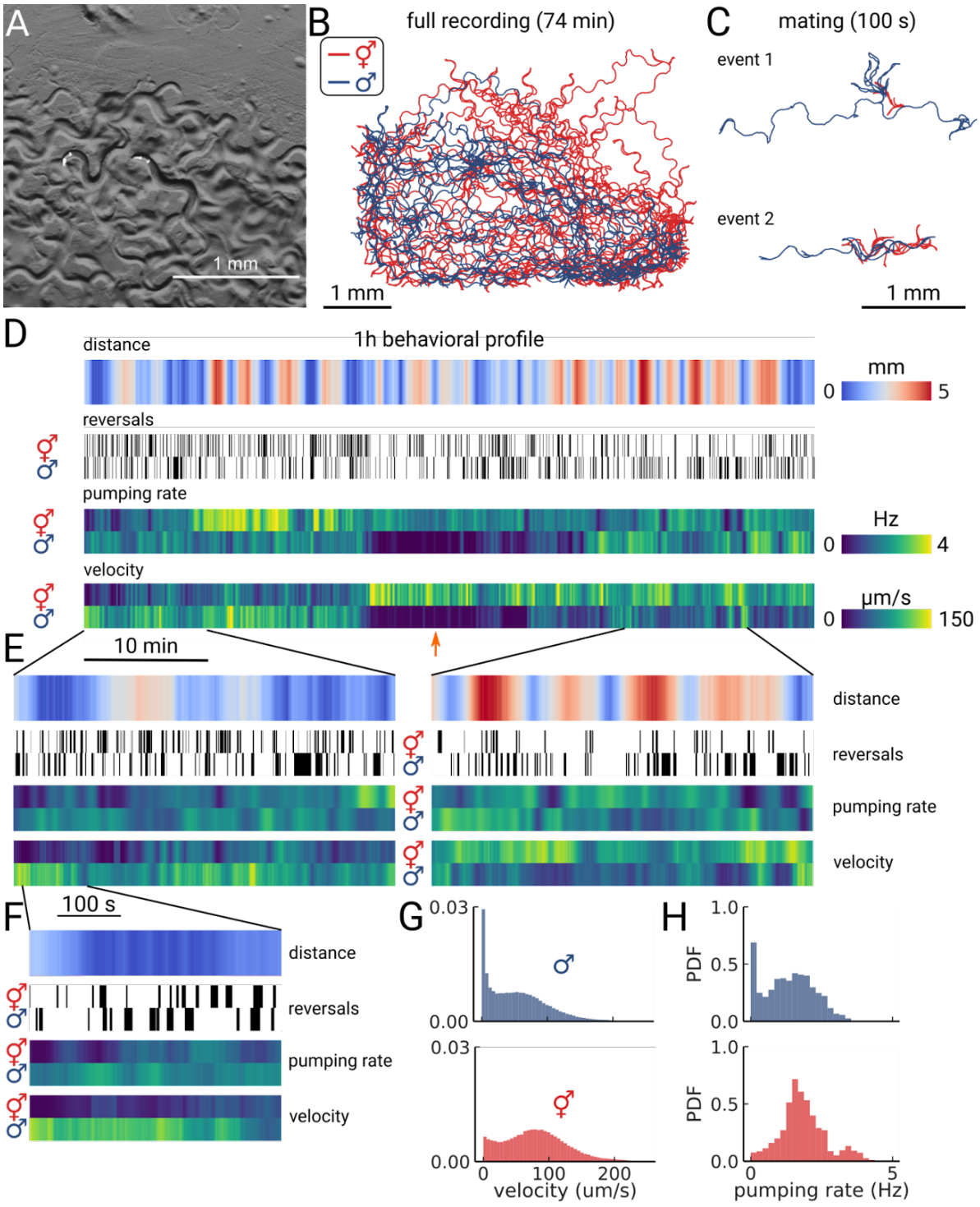

Figure 5 Long-term imaging of mating animals

(A) Composite image of the two animals in the arena while exposed to bright-field illumination and exciting fluorescence of YFP using green light. On the right, the hermaphrodite, on the left the male identifiable by its smaller size and its tail with sensory rays and fan. (B) Trajectories obtained from the full recording of the male (blue) and hermaphrodite (red). (C) Example mating events. (D) Behavioral measures for 1h of data. The distance between the animals, the reversal events, pumping rate, and velocity are shown for the hermaphrodite and the male. The male shows an extended period of quiescence (orange arrow). (E) Behavioral measures for 10 minutes of data and (F) 100 s of data corresponding to the mating event 1 in panel (C). (G) Velocity distribution and (H) pumping rate distribution for the male and hermaphrodite.

6. Limitations and requirements

Using a combination of low-magnification fluorescence imaging and dedicated analysis software, we show that it is possible to perform high-throughput, automated pumping detection of worms crawling on standard culture plates. There are some limitations to the method that are due to the reliance on a fluorescent indicator in the pharyngeal muscle and the handling of the large datasets that are generated. We find that uneven plates or improper focus leads to low signal-to-noise ratios. With careful focusing, imaging the center of evenly poured plates and using our custom peak detection method that is adaptive to the image quality (see Methods), these pitfalls can be mediated. Additionally, once at focus, small variations of the worm height do not affect the result, as low-magnification imaging results in a large depth of field.

As it is necessary for our approach to label the pharynx, mutant characterization with our tool would require crossing all possible mutants with a fluorescent reporter strain, and albeit labor intensive this is nonetheless still a standard genetic practice when a reporter is used. While most experiments in this paper were performed with a homozygous, integrated reporter background (*gnals1*), we have also used extrachromosomal arrays with success (Fig. S3.4), which allows the use of animals that have a *myo-2* reporter as a co-injection marker, for example. In addition, since our tool relies on the detection of fluorescent protein, siblings losing the transgene on the plate will not interfere with the analysis.

To maximize the field-of-view, we have chosen the smallest spatial resolution at which we could reliably detect pumping in wildtype adults. To ensure detection in smaller animals, increasing the magnification in these cases is recommended, as we did to detect pumping in larvae. The final requirement is related to data management and handling. While the hardware requirements are restricted to equipment commonly available in many laboratories (a fluorescence dissecting microscope and a Megapixel camera are needed), the data rate of the large area scan cameras is > 6GB/s. On a 4-core laptop, the expected analysis time is approximately 8 h for 150 worm-minutes of data. While the analysis can be run on a laptop or desktop computer, runtime is much improved when using a computing cluster (see Supplementary materials).

Discussion

We developed a microscopy protocol and customized image analysis software that enables simultaneous measurements of locomotion and feeding in unrestrained animals. We are able to accurately detect pumping rates in populations of animals on plates at single-worm, single-pump resolution. Our fully automatic method provides an increase in throughput by more than one order of magnitude, and does not require any laborious handling of the animals or microfluidic devices. As our imaging does not adversely affect worms, animals can be imaged multiple times, as we demonstrated by following pumping in a population of developing animals or can be imaged continuously for hours as shown for the mating animals. In addition, by enabling measurements of unrestrained animals directly on agarose plates, our

approach creates opportunities for studying novel behaviors, such as foraging in complex environments [32,60] or behavioral coordination [27,61].

Using our method, we were able to detect quiescent episodes in all four larval stages that were absent in the young adult. It will be interesting to study the food needs at different stages and how feeding is regulated on the scale of minutes. To understand the neural basis of feeding, resolving the decisions underlying feeding behavior is required [9,13]. However, current bulk methods capable of extracting population averages of pumping rates are insufficient to understand underlying neural activity, as the data lack the temporal resolution to correlate pumping with neural activity. Additionally, it is desirable to image animals in their normal culturing environments to compare feeding behaviors to established baselines e.g., for velocity and reversals. Our method enables the quantification of pumping activity, in multiple animals simultaneously, as a marker of feeding behavior in *C. elegans*.

An essential requirement for the broad applicability of such a tool is its use for genetic and pharmacological screens. We demonstrated the suitability of our tool for studying the pumping and locomotory behaviors of *unc-31* and *eat-18* animals. We could identify a bimodal distribution of pumping rates for *unc-31* mutants with some showing low rates for the duration of the recording. This indicates that while these animals are capable of fast pumping, they do not show the same temporal regulation as N2 animals, which show rapid transitions between slow and fast pumping, and pump fast most of the time at high food levels [9]. We could also reveal a previously unreported alteration in pump duration for *eat-18* animals. Surprisingly, during confirmation of the feeding defect, we also discovered a previously unreported locomotion defect, hinting at a broader function for *eat-18* possibly outside of the pharynx.

Additionally, PharaGlow enables easy pharmacological screens on plates, by allowing experimenters to directly apply compounds to culture plates without requiring microfluidics or immobilization. Immobilization often requires the addition of serotonin (5-HT) to stimulate pumping, as pumping is suppressed in restrained animals [28]. It is likely that observed feeding defects differ between crawling, food-stimulated animals and serotonin-stimulated animals [7] , and that new experiments will be effective in identifying phenotypes that went unnoticed in immobilized preparations.

To mimic realistic foraging situations would require extending the foraging arena by supplying variable patches of food, and providing a more interesting landscape rather than a homogenous 2D plate environment. Patch foraging has been extensively studied in *C. elegans*, both with respect to entry into single patches [13,60,62] and food choice [13,63,64], though these studies focused on locomotion rather than pumping rates. Testing models of patch foraging and their predictions [65] while explicitly including measured food intake will help better define the limits in which simple models of foraging are applicable. Moreover, this would ideally expand our understanding of the underlying strategies learned or inherited by worms living in different environments. Technically, current imaging limitations , such as the field of view, can be

extended by using larger camera arrays, which will enable scanning across multiple centimeter-sized fields of view. These experiments would also require long-term imaging of the animals to observe transitions between food patches, which is possible using our method.

A further extension of this work would be to image pumping activity in related species, either *Caenorhabditis* nematodes collected from different field sites, or even predatory nematodes like *Pristionchus pacificus,* which has a bacterial feeding mode similar to *C. elegans* and additionally a predatory mode when killing the larvae of other nematodes. While the requirement for labeling the muscle is a prerequisite of our method, the *myo-2* gene is a myosin heavy chain that is conserved among nematodes and will likely show similar expression in closely related species. A strain with the *myo-2* promoter construct for the closely related *C. briggsae* is already available at the CGC. Our tool opens new venues to study feeding behaviors at multiple scales. We envision that its application will lead to new insights into worm behavior.

Methods

Key Resources Table				
Reagent type (species) or resource	**Designation**	**Source or reference**	**Identifiers**	**Additional information**
strain, strain background (*Escherichia coli* OP50)	OP50	CGC	CGC:OP50	
Recombinant DNA reagent	*myo-2p::mCherry::unc-54 3'utr*	Addgene	pCFJ90	5ng/ul injected into N2
Recombinant DNA reagent	*pPHA2::GFP-F*	Gift from Marc Pilon	pMS17	50 ng/ul injected into N2
strain, strain background (*C. elegans*)	N2	CGC	N2	Background for INF30
strain, strain background (*C. elegans*)	*gnaIs1[myo-2p::yfp]*	CGC	GRU101	
strain, strain background (*C. elegans*)	*nonEx9*[*pPHA2::GFP-F myo-2p::mCherry::unc-54 3'utr*]	This publication	INF30	5ng/ul of pMS17 and 5 ng/ul of pCFJ90 injected into N2
strain, strain background (*C. elegans*)	*unc-31(e928) gnaIs1 IV*	This publication	INF5	Cross of *unc-31(e928)* with GRU101
strain, strain background (*C. elegans*)	*unc-31(n1304) gnaIs1 IV*	This publication	INF17	Cross of *unc-31(n1304)* with GRU101
strain, strain background (*C. elegans*)	*eat-18(ad820) I; gnaIs1 IV*	This publication	INF44	Cross of *eat-18(ad820)* with GRU101
software, algorithm	PharaGlow	This publication		

***C. elegans* maintenance**

C. elegans were grown on NGM plates at 20°C. Worms were synchronized by letting adult gravid animals lay eggs for 2-3 h, then removing the adults. The average time from egg to young adult stage for strain GRU101 (*gnaIs1[myo-2p::yfp])* was 63h. Before the experiment, synchronized adults were washed off the culture plates with 1 ml of M9 and collected in an Eppendorf tube. Worms were allowed to settle for 1 min, the supernatant was removed and the tube was refilled with M9. Washing was repeated two more times. The washing was sufficient in that we did not observe animals remaining in the spots containing the remainder of M9 on the assay plates, suggesting that the bacterial amount was too diluted to induce dwelling behavior.

Strains

Strain	**Genotype**	**Figures (Panels)**	**Source**
GRU101	*gnaIs1[myo-2p::yfp]*	All	CGC
INF30	*nonEx9[pPHA2::GFP-F; myo-2p::mCherry::unc-54 3'utr]*	Fig.2.4	This publication
INF5	*unc-31(e928) gnaIs1 IV*	Fig. 3	This publication
INF17	*unc-31(n1304) gnaIs1 IV*	Fig. 3	This publication
INF44	*eat-18(ad820) I; gnaIs1 IV*	Fig. 3	This publication

Imaging setup

Imaging of worms at 1x magnification was performed using a commercial upright epifluorescence microscope (Axio Zoom V16; Zeiss) equipped with a 1x objective (PlanNeoFluar Z 1.0x/N.A. 0.25). For imaging of YFP fluorescence, light from an LED lamp (X-Cite XYLIS) was reflected towards the sample using a dichroic mirror (FT 515; Zeiss) and filtered (BP 500/25; Zeiss). Emitted light was filtered using a band-pass filter (BP 535/30; Zeiss) and focused onto the camera sensor (acA3088-57um; BASLER) using a camera adapter with an additional 0.5x magnification (60N-C ⅔" 0.5x; Zeiss). The power density of fluorescence excitation at the focal plane (0.24 mW/mm^2 at 500 nm) was measured using a power meter sensor (PS19Q; Coherent) with the corresponding controller (PowerMax; Coherent). Animals were imaged at 30 fps for 5 minutes unless otherwise indicated. For imaging of mCherry, the filter cube was replaced with a commercial filter set (64 HE; Zeiss). The resulting power density using this cube was 0.76 mW/mm^2 at the focal plane.

Long-term imaging

For long-term imaging, stroboscopic illumination (5 ms light pulses) were used to reduce bleaching. Excitation light was synchronized with the camera exposure using the GPIO camera line and the TTL input of the LED lamp. Frames were collected using a custom software (LabVIEW; software will be made

available upon publication). To reduce the amount of stored data and allow continuous recording using a standard computer (Celsius W520; Fujitsu), images were segmented automatically and only areas containing worms, and their coordinates within the image, were stored. This procedure allowed a data reduction by approximately 1,000 fold. For imaging, a copper frame (5.3 x 3.75 x 1 mm) was filled with 2% low melting point agarose (Sigma Aldrich) in M9 and 5 µl of a 10-fold concentrated overnight OP50 culture was seeded on top. The frame was deposited into a 10 cm NGM plate, and worms were transferred to the agarose arena. To preserve the moisture of the preparation and prevent shrinking of the gel, about ⅓ of the agar at the outer rim of the plate was removed using a scalpel and the space was filled with 6 ml of M9.

Dual bright-field and fluorescence imaging

Dual imaging was performed using an upright microscope (BX51WI; Olympus) and a 10x objective (UplanSApo, NA 0.4; Olympus). For bright-field imaging, light emanating from a near-infrared (780 nm) LED (M780LP1 and driver LEDD1B; Thorlabs) was filtered using a (785/62 BrightLine HC; Semrock) and projected onto the sample via the bright-field illumination condenser. To excite fluorescence, the Teal line from an LED lamp (Spectra X light engine; Lumencor) was filtered (513/17 BrightLine HC; Semrock) and projected onto the sample using a 520 nm long-pass dichroic (FF520-Di02; Semrock). Transmitted and emitted light were filtered using a 532 long-pass filter (BLP01-532R; Semrock). To simultaneously record images in bright-field and fluorescence, a dual-camera device was used (DC^2; Photometrics). Light was split into two channels using a 695 long-pass dichroic mirror (695DCXRUV; Photometrics) and images were projected into two cameras (acA3088-57um; BASLER). Fluorescent light was band-pass filtered (550/49 Brightline HC; Semrock) before reaching the camera sensor. The exposure time (6 ms) of one camera served to synchronize the acquisition of the second camera and the Lumencor light engine. Individual worms were manually tracked using a 3-axis motorized stage (X-LSM150A; Zaber).

Developmental pumping experiments

Worms were pre-synchronized by hypochlorite bleaching, allowed to hatch overnight in M9 and then cultured on NGM plates with OP50 at 20°C. On day 3 after pre-synchronization, worms were synchronized again by letting 20 gravid animals lay eggs for 2 h per assay plate, then removing the adults and letting embryos grow for specific durations to reach the appropriate larval or adult stage (19 h for mid-L1, 31 h for mid-L2, 39 h for mid-L3, 50 h for mid-L4, 65 h for young adults). For the assay plates, 40 µl of *E. coli* OP50 culture was spotted onto an empty 6 cm NGM plate a few hours before the synchronization and left to dry. Synchronized worms were imaged directly on their assay plates as described in section “Imaging setup”. The magnification for each stage was chosen to achieve an approximate pharynx length of ~60 pixels (2x (1.18 µm/px) for L1, 1.5x (1.57 µm/px) for L2, 1.4x (1.69 µm/px) for L3, 1.3x (1.81 µm/px) for L4 and the standard 1x (2.36 µm/px) for young adults). 3 assay plates were imaged once per stage, and 3 additional plates were imaged at each stage to test for photo-sensitivity.

Starvation experiments

Washed animals were transferred to the center of an empty 6 cm NGM plate at room temperature and left to recover for 15 minutes before imaging.The same plate was imaged at defined time points for progressively more starved animals (at 30 min, 90 min, 150 min and 210 min after being taken off food). The field of view was chosen randomly on the plate but was required to contain at minimum 3 worms at the beginning of the recording. For control, washed animals were transferred close to a 40 µl of *E. coli* OP50 lawn, which was spotted onto an empty 6 cm NGM plate a few hours before the recordings and allowed to dry. Acclimation time and recording are similar for starved animals.

Automated Analysis

Pharyngeal pumping - fluorescence data

Animals were tracked using our custom python analysis package ***PharaGlow*** which is freely available under a permissive GPL 3.0 license. In brief, PharaGlow runs a three-step analysis: 1. center of mass tracking and collision detection, 2. linking detected objects to trajectories and 3. extracting centerline, contour, width, and other parameters of the shape to allow extracting pharyngeal pumping events. Tracking uses the soft matter package [66]. The code is fully modular and any existing tracking code could in principle be used for the first two steps provided the input data is formatted to PharaGlow standards. We provide example data and example jupyter notebooks to help users make use of our package both in personal computer and high-performance cluster settings. The resulting files contain the position, and the straightened images which are further processed to extract the behavioral measures as described in Fig.1 and section '*Pharyngeal pumping - postprocessing*". '

Pharyngeal pumping - postprocessing

To obtain pumping traces from straightened animals, the inverted maximum of the dorso-ventral standard deviation of brightness is calculated for each straightened frame per animal (Fig. 1E). This metric is sensitive to the opening of the pharyngeal lumen and terminal bulb contractions. Peaks in the resulting trace correspond to pumping events. Due to the animal motion, uneven illumination or defocusing can modify the baseline of the pumping metric. We correct for baseline fluctuations and spurious fluorescence changes by subtracting the background fluctuations using a rolling mean filter of 1 s (except for *eat-18* mutants, where we use 3 s otherwise the slow contractions were removed too). To the remaining signal we apply a smoothing filter of width = 66 ms (2 frames). We detect peaks using AMPD, an algorithm for peak detection in quasi-periodic signals [67]. We also require the peak distances to obey physiologically reasonable rates i.e., the peaks can not be closer than $dmin$ = 132 ms (4 frames). To automatically establish the noise level of the trace, we compare the incidence of intervals between detected peaks that violate the assumption $dmin$ >132 ms and select the minimal prominence required, such that the fraction of violating intervals is lower than a sensitivity parameter s. For all dataset with 5 minute recordings, we set $s = 0.999$. In the long-term recordings, we use a hampel filter with a width of 300 frames to remove spurious outliers in the signal which affect peak detection and set $s = 0.9999$.

Depending on the purpose, pumping rates have been calculated as follows: To determine the average pumping rate per track, we calculate the number of pumping events/ total track duration (e.g., Fig 3F, box plots). To obtain pumping rate distributions, we calculate the number of pumps in a sliding window of 10 s and combine data from all tracks. The 'instantaneous pumping rate' is defined as $1/\Delta t$ between pumps. We use the instantaneous rate when a higher temporal resolution is desired. Which rate metric is used is indicated in the caption.

Other behavioral parameters

Velocity was calculated from the tracked center of mass of the labeled pharynx. Reversals were calculated based on the angle between the pharynx and the animal's nose tip direction. To avoid spurious reversals, the nose tip trajectories are coarse-grained to 6 Hz, and the angle between the nose tip and pharynx is smoothed with a window of width = 1s (30 frames). Timepoints with angles exceeding 120° were annotated as reversals. Reversals shorter than 0.5 s are removed. The estimation of the pharyngeal area is based on an automated threshold of the pharynx.

Animal selection

All animals that were successfully tracked for at least 60 seconds (Fig. 1,2,3) were included. No other filtering or outlier removal was performed. Due to age synchronization, all animals in the field of view were of similar size in the wildtype experiments. For *eat-18* mutants, the size and developmental stage of the animals were more dispersed and only animals that had the appropriate size for their stage were included (Fig. 4). In the starvation experiments, animals that were successfully tracked for at least 20 seconds were included due to the larger velocity in this condition (Fig. 3).

Manual annotation of pumping behavior

Movies for individual animals were created from a large field of view and expert annotators counted pumps by displaying the movie using the cell counter tool in Fiji [68]. The annotators were blinded to the movie conditions and to the other experts' results.

Acknowledgments

We thank James Lightfoot and Shawn Lockery for helpful comments. We wish to acknowledge Omar Valerio Minero (MPINB HPC) for assistance with benchmarking. Some strains were provided by the CGC, which is funded by NIH Office of Research Infrastructure Programs (P40 OD010440). Some figure panels were created with biorender.com. We thank Marc Pilon for giving us a plasmid.

Data and Code availability statement

The data from this manuscript is available at https://osf.io/fy4ed/. The Code repository for the PharaGlow package can be found at https://github.com/scholz-lab/PharaGlow.

References

1. Fontana, L. & Partridge, L. Promoting health and longevity through diet: from model organisms to humans. *Cell* **161**, 106–118 (2015).
2. Trepanowski, J. F., Canale, R. E., Marshall, K. E., Kabir, M. M. & Bloomer, R. J. Impact of caloric and dietary restriction regimens on markers of health and longevity in humans and animals: a summary of available findings. *Nutr. J.* **10**, 107 (2011).
3. Balasubramanian, P., Howell, P. R. & Anderson, R. M. Aging and Caloric Restriction Research: A Biological Perspective With Translational Potential. *EBioMedicine* **21**, 37–44 (2017).
4. Avery, L. & Horvitz, H. R. Effects of starvation and neuroactive drugs on feeding in Caenorhabditis elegans. *J. Exp. Zool.* **253**, 263–270 (1990).
5. You, Y.-J., Kim, J., Cobb, M. & Avery, L. Starvation activates MAP kinase through the muscarinic acetylcholine pathway in Caenorhabditis elegans pharynx. *Cell Metab.* **3**, 237–245 (2006).
6. You, Y.-J., Kim, J., Raizen, D. M. & Avery, L. Insulin, cGMP, and TGF-beta signals regulate food intake and quiescence in C. elegans: a model for satiety. *Cell Metab.* **7**, 249–257 (2008).
7. Lee, K. S. *et al.* Serotonin-dependent kinetics of feeding bursts underlie a graded response to food availability in C. elegans. *Nat. Commun.* **8**, 14221 (2017).
8. Song, B.-M. & Avery, L. Serotonin activates overall feeding by activating two separate neural pathways in Caenorhabditis elegans. *J. Neurosci.* **32**, 1920–1931 (2012).
9. Scholz, M., Dinner, A. R., Levine, E. & Biron, D. Stochastic feeding dynamics arise from the need for information and energy. *Proc. Natl. Acad. Sci. U. S. A.* **114**, 9261–9266 (2017).
10. Kang, C. & Avery, L. The FMRFamide Neuropeptide FLP-20 Acts as a Systemic Signal for Starvation Responses in Caenorhabditis elegans. *Mol. Cells* **44**, 529–537 (2021).
11. Srinivasan, S. *et al.* Serotonin regulates C. elegans fat and feeding through independent molecular mechanisms. *Cell Metab.* **7**, 533–544 (2008).
12. Hobson, R. J. *et al.* SER-7, a Caenorhabditis elegans 5-HT7-like receptor, is essential for the 5-HT stimulation of pharyngeal pumping and egg laying. *Genetics* **172**, 159–169 (2006).
13. Katzen, A. *et al.* The nematode worm C. elegans chooses between bacterial foods exactly as if maximizing economic utility. *bioRxiv* 2021.04.25.441352 (2021) doi:10.1101/2021.04.25.441352.

14. Shtonda, B. B. & Avery, L. Dietary choice behavior in Caenorhabditis elegans. *J. Exp. Biol.* **209**, 89–102 (2006).
15. Seymour, M. K., Wright, K. A. & Doncaster, C. C. The action of the anterior feeding apparatus of Caenorhabditis elegans (Nematoda: Rhabditida). *J. Zool.* **201**, 527–539 (1983).
16. Avery, L. & Shtonda, B. B. Food transport in the C. elegans pharynx. *J. Exp. Biol.* **206**, 2441–2457 (2003).
17. Fang-Yen, C., Avery, L. & Samuel, A. D. T. Two size-selective mechanisms specifically trap bacteria-sized food particles in Caenorhabditis elegans. *Proc. Natl. Acad. Sci. U. S. A.* **106**, 20093–20096 (2009).
18. Albertson, D. G. & Thomson, J. N. The pharynx of Caenorhabditis elegans. *Philos. Trans. R. Soc. Lond. B Biol. Sci.* **275**, 299–325 (1976).
19. Trojanowski, N. F., Raizen, D. M. & Fang-Yen, C. Pharyngeal pumping in Caenorhabditis elegans depends on tonic and phasic signaling from the nervous system. *Sci. Rep.* **6**, 22940 (2016).
20. Scholz, M., Lynch, D. J., Lee, K. S., Levine, E. & Biron, D. A scalable method for automatically measuring pharyngeal pumping in C. elegans. *J. Neurosci. Methods* **274**, 172–178 (2016).
21. Song, B.-M., Faumont, S., Lockery, S. & Avery, L. Recognition of familiar food activates feeding via an endocrine serotonin signal in Caenorhabditis elegans. *Elife* **2**, e00329 (2013).
22. Gruninger, T. R., Gualberto, D. G., LeBoeuf, B. & Garcia, L. R. Integration of male mating and feeding behaviors in Caenorhabditis elegans. *J. Neurosci.* **26**, 169–179 (2006).
23. Raizen, D. M., Lee, R. Y. & Avery, L. Interacting genes required for pharyngeal excitation by motor neuron MC in Caenorhabditis elegans. *Genetics* **141**, 1365–1382 (1995).
24. McKay, J. P., Raizen, D. M., Gottschalk, A., Schafer, W. R. & Avery, L. eat-2 and eat-18 are required for nicotinic neurotransmission in the Caenorhabditis elegans pharynx. *Genetics* **166**, 161–169 (2004).
25. Raizen, D. M. & Avery, L. Electrical activity and behavior in the pharynx of Caenorhabditis elegans. *Neuron* **12**, 483–495 (1994).
26. Li, Z. *et al.* Dissecting a central flip-flop circuit that integrates contradictory sensory cues in C. elegans feeding regulation. *Nat. Commun.* **3**, 776 (2012).
27. Cermak, N. *et al.* Whole-organism behavioral profiling reveals a role for dopamine in state-dependent motor program coupling in C. elegans. *Elife* **9**, (2020).

28. Takahashi, M. & Takagi, S. Optical silencing of body wall muscles induces pumping inhibition in Caenorhabditis elegans. *PLoS Genet.* **13**, e1007134 (2017).
29. Izquierdo, P. G. *et al.* Cholinergic signaling at the body wall neuromuscular junction distally inhibits feeding behavior in Caenorhabditis elegans. *J. Biol. Chem.* **298**, 101466 (2022).
30. Ramot, D., Johnson, B. E., Berry, T. L., Jr, Carnell, L. & Goodman, M. B. The Parallel Worm Tracker: a platform for measuring average speed and drug-induced paralysis in nematodes. *PLoS One* **3**, e2208 (2008).
31. Swierczek, N. A., Giles, A. C., Rankin, C. H. & Kerr, R. A. High-throughput behavioral analysis in C. elegans. *Nat. Methods* **8**, 592–598 (2011).
32. Ding, S. S., Romenskyy, M., Sarkisyan, K. S. & Brown, A. E. X. Measuring Caenorhabditis elegans Spatial Foraging and Food Intake Using Bioluminescent Bacteria. *Genetics* **214**, 577–587 (2020).
33. Andersen, E. C., Bloom, J. S., Gerke, J. P. & Kruglyak, L. A variant in the neuropeptide receptor npr-1 is a major determinant of Caenorhabditis elegans growth and physiology. *PLoS Genet.* **10**, e1004156 (2014).
34. Kiyama, Y., Miyahara, K. & Ohshima, Y. Active uptake of artificial particles in the nematode Caenorhabditis elegans. *J. Exp. Biol.* **215**, 1178–1183 (2012).
35. Gomez-Amaro, R. L. *et al.* Measuring Food Intake and Nutrient Absorption in Caenorhabditis elegans. *Genetics* **200**, 443–454 (2015).
36. Zou, W. *et al.* Decoding the intensity of sensory input by two glutamate receptors in one C. elegans interneuron. *Nat. Commun.* **9**, 4311 (2018).
37. Lockery, S. R. *et al.* A microfluidic device for whole-animal drug screening using electrophysiological measures in the nematode C. elegans. *Lab Chip* **12**, 2211–2220 (2012).
38. Rodríguez-Palero, M. J. *et al.* An automated method for the analysis of food intake behaviour in Caenorhabditis elegans. *Sci. Rep.* **8**, 3633 (2018).
39. Dallière, N. *et al.* Multiple excitatory and inhibitory neural signals converge to fine-tune Caenorhabditis elegans feeding to food availability. *FASEB J.* **30**, 836–848 (2016).
40. Bhatla, N., Droste, R., Sando, S. R., Huang, A. & Horvitz, H. R. Distinct Neural Circuits Control Rhythm Inhibition and Spitting by the Myogenic Pharynx of C. elegans. *Curr. Biol.* **25**, 2075–2089 (2015).

41. Okkema, P. G., Harrison, S. W., Plunger, V., Aryana, A. & Fire, A. Sequence requirements for myosin gene expression and regulation in Caenorhabditis elegans. *Genetics* **135**, 385–404 (1993).

42. Okkema, P. G. & Fire, A. The Caenorhabditis elegans NK-2 class homeoprotein CEH-22 is involved in combinatorial activation of gene expression in pharyngeal muscle. *Development* **120**, 2175–2186 (1994).

43. Knight, C. G., Patel, M. N., Azevedo, R. B. R. & Leroi, A. M. A novel mode of ecdysozoan growth in Caenorhabditis elegans. *Evol. Dev.* **4**, 16–27 (2002).

44. Gallagher, T., Kim, J., Oldenbroek, M., Kerr, R. & You, Y.-J. ASI regulates satiety quiescence in C. elegans. *J. Neurosci.* **33**, 9716–9724 (2013).

45. Davis, K. C., Choi, Y.-I., Kim, J. & You, Y.-J. Satiety behavior is regulated by ASI/ASH reciprocal antagonism. *Sci. Rep.* **8**, 6918 (2018).

46. Chalfie, M. *et al.* The neural circuit for touch sensitivity in Caenorhabditis elegans. *J. Neurosci.* **5**, 956–964 (1985).

47. Zhao, B., Khare, P., Feldman, L. & Dent, J. A. Reversal frequency in Caenorhabditis elegans represents an integrated response to the state of the animal and its environment. *J. Neurosci.* **23**, 5319–5328 (2003).

48. Chiba, C. M. & Rankin, C. H. A developmental analysis of spontaneous and reflexive reversals in the nematode Caenorhabditis elegans. *J. Neurobiol.* **21**, 543–554 (1990).

49. Dillon, J., Holden-Dye, L., O'Connor, V. & Hopper, N. A. Context-dependent regulation of feeding behaviour by the insulin receptor, DAF-2, in Caenorhabditis elegans. *Invert. Neurosci.* **16**, 4 (2016).

50. Gray, J. M., Hill, J. J. & Bargmann, C. I. A circuit for navigation in Caenorhabditis elegans. *Proc. Natl. Acad. Sci. U. S. A.* **102**, 3184–3191 (2005).

51. Scholz, M., Lynch, D. J., Lee, K. S., Levine, E. & Biron, D. A scalable method for automatically measuring pharyngeal pumping in C. elegans. *J. Neurosci. Methods* **274**, 172–178 (2016).

52. Keane, J. & Avery, L. Mechanosensory inputs influence Caenorhabditis elegans pharyngeal activity via ivermectin sensitivity genes. *Genetics* **164**, 153–162 (2003).

53. Hills, T., Brockie, P. J. & Maricq, A. V. Dopamine and glutamate control area-restricted search behavior in Caenorhabditis elegans. *J. Neurosci.* **24**, 1217–1225 (2004).

54. Sawin, E. R., Ranganathan, R. & Horvitz, H. R. C. elegans locomotory rate is modulated by the environment through a dopaminergic pathway and by experience through a serotonergic pathway. *Neuron* **26**, 619–631 (2000).

55. Calhoun, A. J., Chalasani, S. H. & Sharpee, T. O. Maximally informative foraging by Caenorhabditis elegans. *Elife* **3**, e04220 (2014).

56. Wakabayashi, T., Kitagawa, I. & Shingai, R. Neurons regulating the duration of forward locomotion in Caenorhabditis elegans. *Neurosci. Res.* **50**, 103–111 (2004).

57. Avery, L., Bargmann, C. I. & Horvitz, H. R. The Caenorhabditis elegans unc-31 gene affects multiple nervous system-controlled functions. *Genetics* **134**, 455–464 (1993).

58. Choudhary, S. *et al.* EAT-18 is an essential auxiliary protein interacting with the non-alpha nAChR subunit EAT-2 to form a functional receptor. *PLoS Pathog.* **16**, e1008396 (2020).

59. Mörck, C. & Pilon, M. C. elegans feeding defective mutants have shorter body lengths and increased autophagy. *BMC Dev. Biol.* **6**, 39 (2006).

60. Iwanir, S. *et al.* Serotonin promotes exploitation in complex environments by accelerating decision-making. *BMC Biol.* **14**, 9 (2016).

61. Hardaker, L. A., Singer, E., Kerr, R., Zhou, G. & Schafer, W. R. Serotonin modulates locomotory behavior and coordinates egg-laying and movement in Caenorhabditis elegans. *J. Neurobiol.* **49**, 303–313 (2001).

62. Flavell, S. W. *et al.* Serotonin and the neuropeptide PDF initiate and extend opposing behavioral states in C. elegans. *Cell* **154**, 1023–1035 (2013).

63. Milward, K., Busch, K. E., Murphy, R. J., de Bono, M. & Olofsson, B. Neuronal and molecular substrates for optimal foraging in Caenorhabditis elegans. *Proc. Natl. Acad. Sci. U. S. A.* **108**, 20672–20677 (2011).

64. Dal Bello, M., Pérez-Escudero, A., Schroeder, F. C. & Gore, J. Inversion of pheromone preference optimizes foraging in C. elegans. *Elife* **10**, (2021).

65. Davidson, J. D. & Hady, A. E. Foraging as an evidence accumulation process. *PLoS Comput. Biol.* **15**, e1007060 (2019).

66. Allan, D. *et al.* soft-matter/trackpy: Trackpy v0. 4.2. *Zenodo, DOI* **10**, (2019).

67. Scholkmann, F., Boss, J. & Wolf, M. An Efficient Algorithm for Automatic Peak Detection in Noisy Periodic and Quasi-Periodic Signals. *Algorithms* **5**, 588–603 (2012).

68. Schindelin, J. *et al.* Fiji: an open-source platform for biological-image analysis. *Nat. Methods* **9**, 676–682 (2012).

69. Ward, A., Liu, J., Feng, Z. & Xu, X. Z. S. Light-sensitive neurons and channels mediate phototaxis in C. elegans. *Nat. Neurosci.* **11**, 916–922 (2008).

70. Bhatla, N. & Horvitz, H. R. Light and hydrogen peroxide inhibit C. elegans Feeding through gustatory receptor orthologs and pharyngeal neurons. *Neuron* **85**, 804–818 (2015).

71. De Magalhaes Filho, C. D. *et al.* Visible light reduces C. elegans longevity. *Nat. Commun.* **9**, 927 (2018).

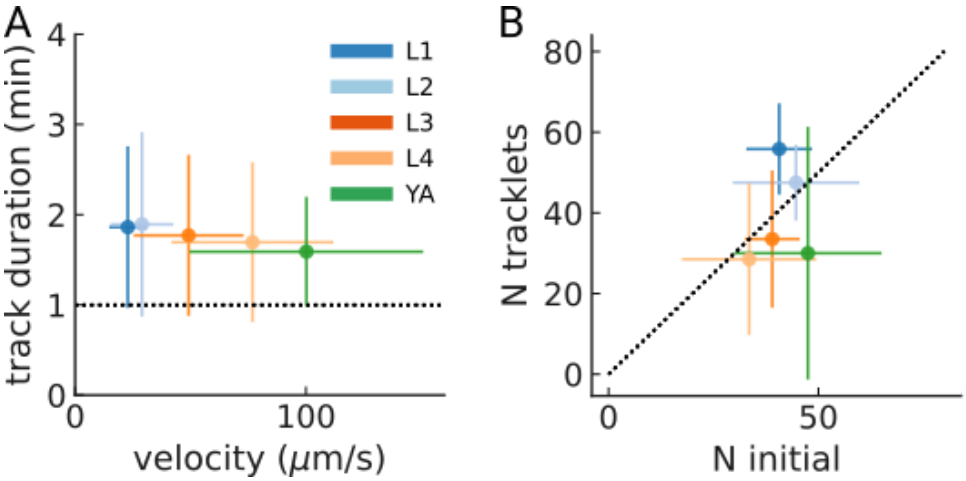

Figure S2.1 Track duration and number of tracked animals per experiment
(A) Mean track duration per experiment across larval stages (N = 6 plates per larval stage). Error bars denote s.d. between plates. (B) Correlation between the number of animals initially in the field of view, and the resulting number of tracks (N = 6 plates per larval stage). The dashed line denotes unity. Error bars denote s.d. between plates.

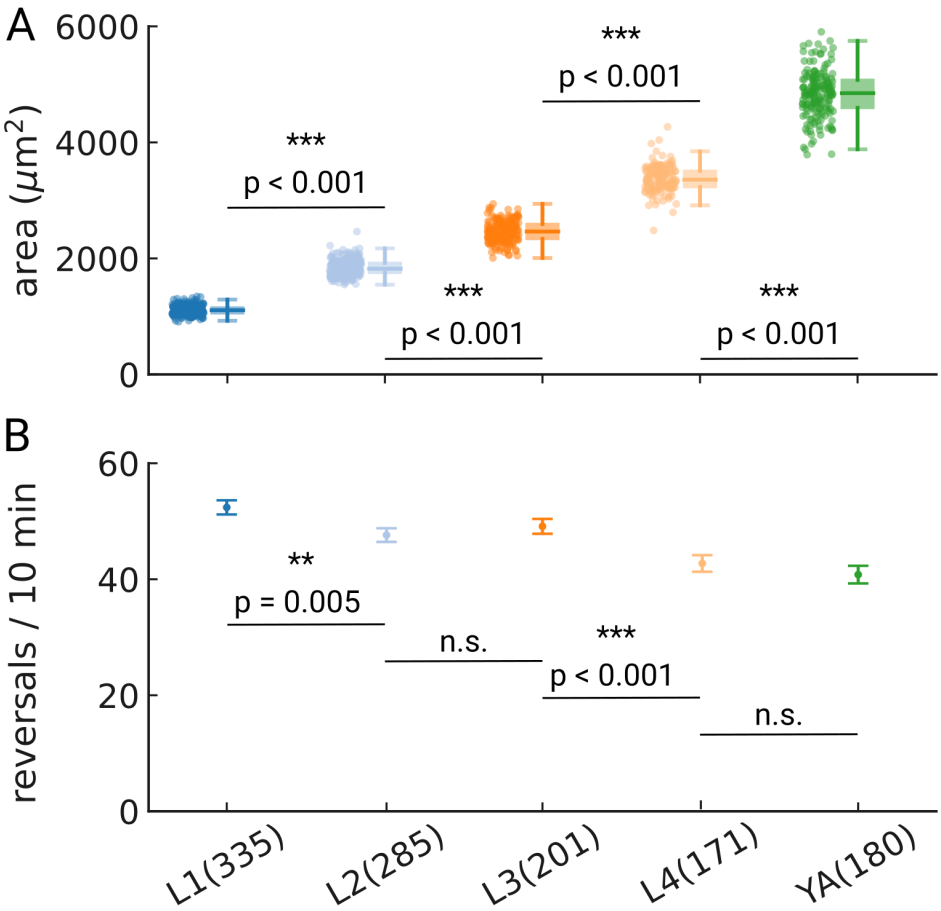

Figure S2.2 Reversal rates across development.
(A) Area of the pharynx as measured by thresholding and segmentation. Sample sizes are given in panel (B). (B) Reversal rates throughout development are detected by comparing the nose-tip motion to the center of mass motion. Rates were rescaled to reversals per 10 minutes to allow comparison to other studies. Error bars denote s.e.m. Significant differences between stages are indicated as ** (p<0.01) and *** (p<0.001), and exact p-values are reported in each panel for all p-values <0.01 (Welch's unequal variance two-tailed t-test). Number of animal tracks is shown in parenthesis.

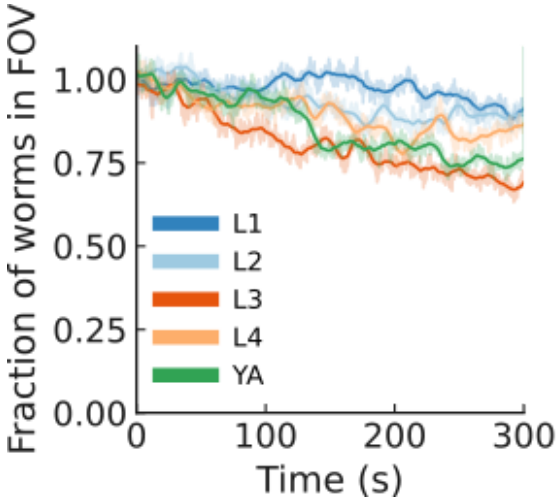

Figure S2.3 Only a mild leaving was induced by light
Mean number of animals in the field of view during the recording. Shaded: average across plates (N = 6 plates per condition), line: smoothed (averaging window = 10 s).

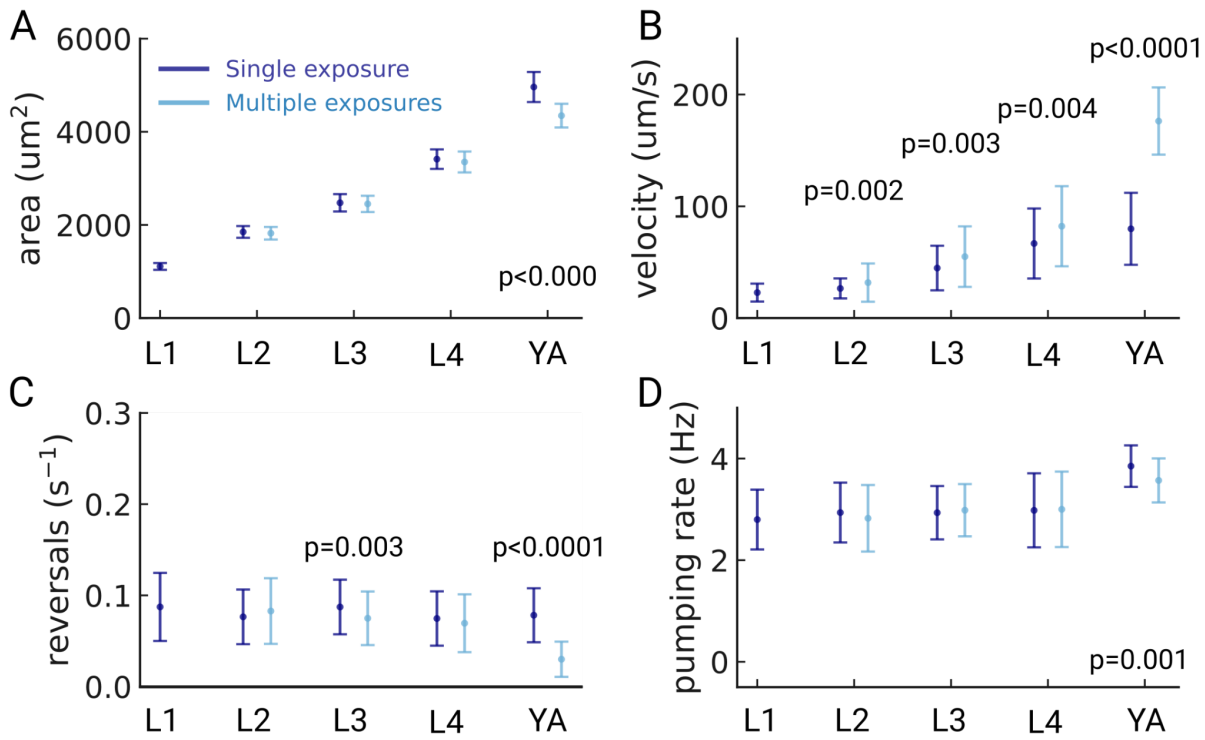

Figure S2.4 Possible light-induced behavioral changes
(A) Pharyngeal area of the detected animals for the group of animals that were imaged once (dark blue) or multiple times (light blue). (B) velocity, (C) reversal rate and (D) pumping rate for the same two cohorts. p-values are reported at the bottom for all p-values <0.01. (Welch's unequal variance two-tailed t-test). The sample size of each group was L1 (191/144), L2 (132/153), L3 (87/114), L4 (112/59) and YA (38/142), for $N_{multiple}$,/N_{Single}, respectively. Significant p-values are explicitly reported in the figure, all other pairwise comparisons were not significant. (Welch's unequal variance two-tailed t-test).

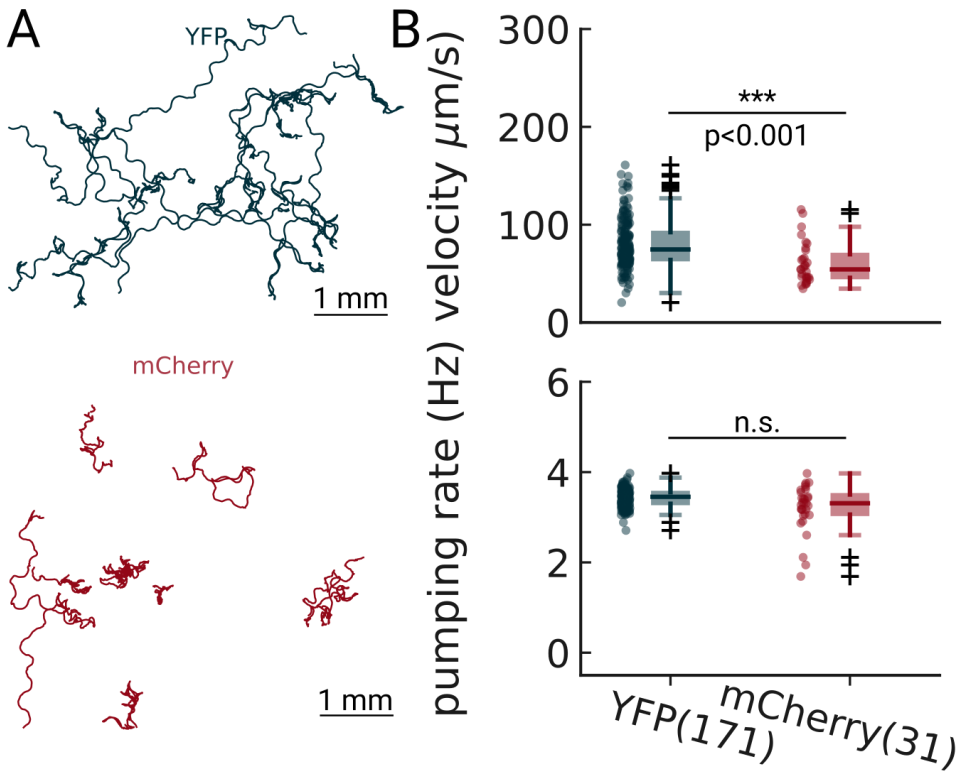

Figure S2.5 Pumping detection is robust at two different excitation wavelengths
Animals expressing either YFP (blue) or mCherry (red) were imaged on food and analyzed using PharaGlow. The pumping rates are not significantly different (Welch's unequal variance two-tailed t-test).

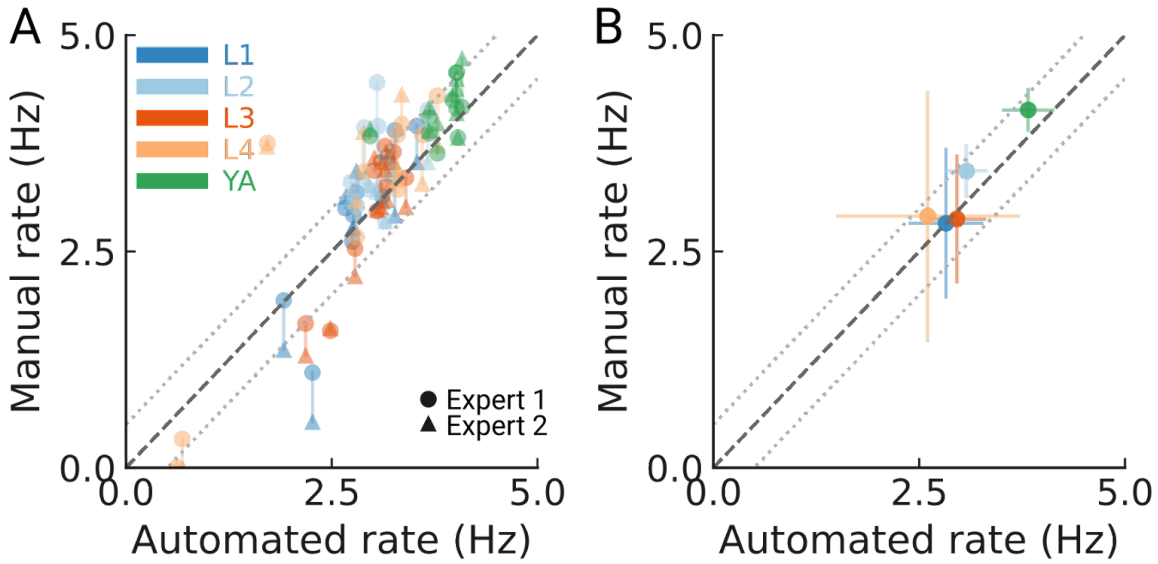

Figure S2.6 Detection accuracy for all developmental stages
(A) Manually counted pumping events for 10 worms per stage (color coded) from two independent experts compared to the automated tracking. Counts of each expert are shown as a circle or triangle. The dashed line indicates unity; the dotted lines denote a 0.5 Hz difference in the resulting pumping rate. (B) The mean pumping rates per developmental stage from the experts and automated method (N = 10 animal tracks per stage). The error bars are s.d. between animal tracks. The two expert counts were averaged to obtain one mean count per animal. The dashed line indicates unity; the dotted lines denote a 0.5 Hz rate difference.

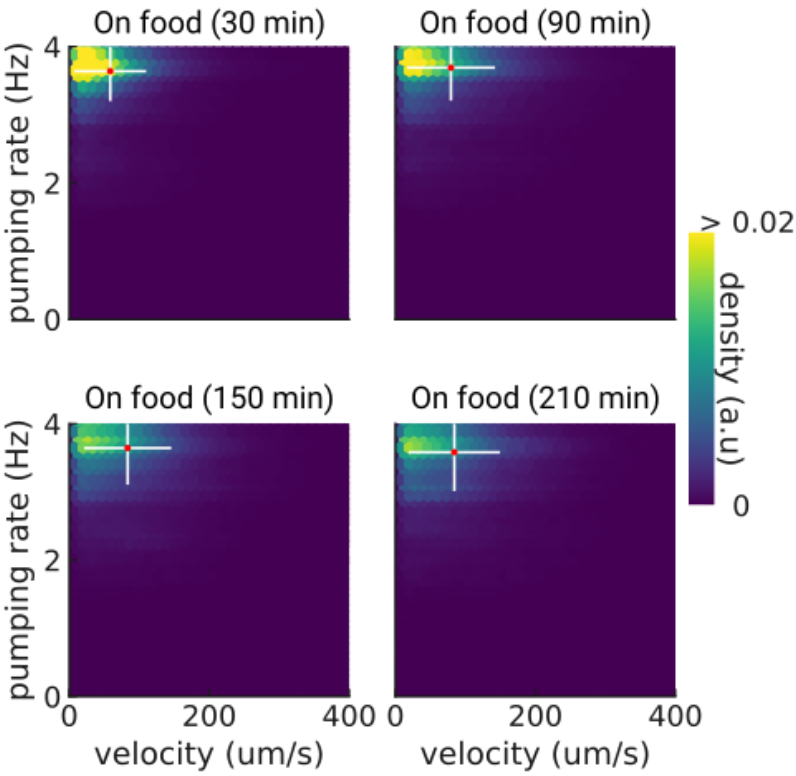

Figure S3.1 Pumping and velocity correlation on food
Correlation between velocity and pumping rate for increasing times on food. The cross indicates the mean (red) and standard deviation (white). The density is normalized by sample number.

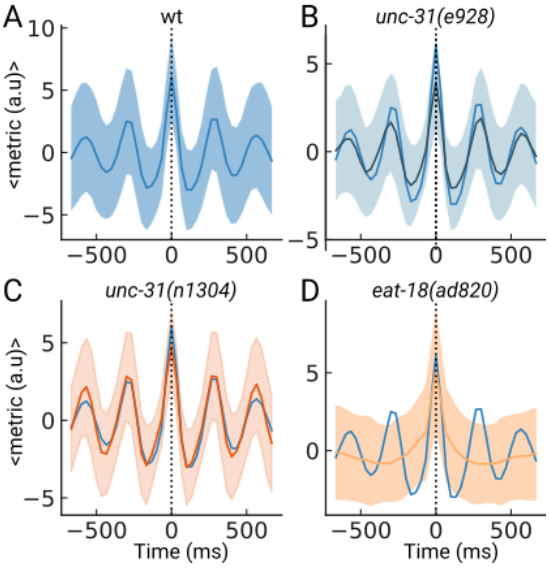

Figure S4.1 Peak-triggered average of the pumping metric.
(A) Average of the pumping metric around the detected peaks of N = 10 randomly selected sample animal tracks. The shaded area denotes the standard deviation. (B), (C), (D) same as (A) but the wildtype peak shape is underlaid in dark blue.

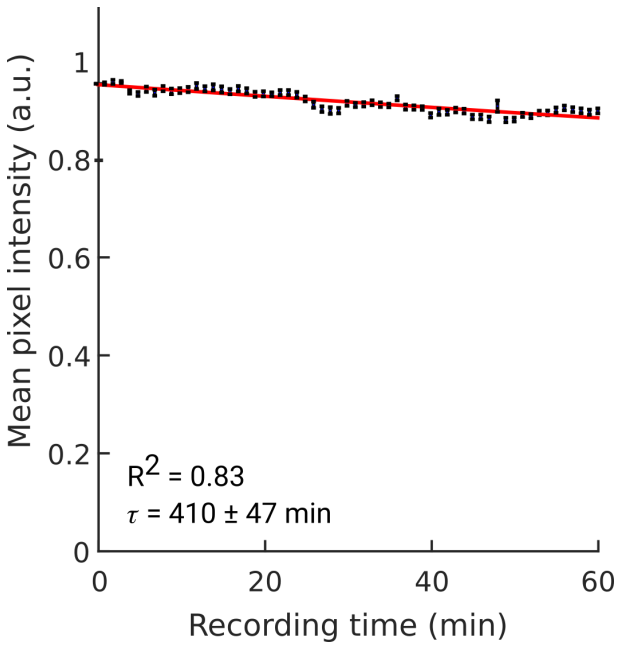

Figure S5.1 Bleaching of YFP.
Bleaching of YFP fluorescence during continuous acquisition at 30 FPS (1x magnification). Stroboscopic illumination was used (5 ms light pulses; see Methods). Average of N = 11 worms. Individual worm bleaching curves were normalized to unity at t = 0. The fit to an exponential decay function yields a decay rate of 410 ± 47 min (95% confidence bounds). Error bars indicate sem across worms.

Supplementary data

Video 1 of a GRU101 worm pumping with the pumping metric shown.

Video 2 Simultaneous bright-field (top-left) and fluorescence imaging (top-right) of a freely moving GRU101 worm at 10x magnification. Downscaled fluorescent images (1x magnification; bottom-left) and resulting pumping events detected by PharaGlow (bottom-right).

Video 3 *eat-18* animal pumping.

Video 4 Live segmentation of worms. The program stores only the segmented worms from individual images and their xyzt coordinates to reduce storage requirements by several orders of magnitude thus allowing uninterrupted recordings for hours at 30 FPS.